Proceeding of the IEEE
International Conference on Robotics and Biomimetics
Dali, China, December 2019

Kinematic Performance and Task Planning Analysis of a Parameter Reconfigurable Parallel Mechanism*

Dian Li
Robotics Institute, School of Mechanical and Electronic Engineering
Beijing Jiaotong University
Beijing 100044, China
15116345@bjtu.edu.cn

Sheng Guo, Yaqiong Chen
Robotics Institute, School of Mechanical and Electronic Engineering
Beijing Jiaotong University
Beijing 100044, China
shguo@bjtu.edu.cn, chenyaqiong@bjtu.edu.cn

***Abstract* - This paper proposed a parameter reconfigurable parallel mechanism (PRPM), which mechanical structure has been introduced. Kinematic performance and task planning analysis has been carried out. DOF of moving platform is calculated based on screw theory in the first place. Then, inverse/forward kinematics, Jacobian matrix and performance indexes, which include dexterity, stiffness, workspace, singularity are analyzed. On the basis of kinematics, task planning analysis is presented. The analysis proposed a method, which is used to acquire appropriate parameters of PRPM according to a specific task. The task workspace can be fulfilled by applying suitable structural angle range of PRPM. Example case is carried out by using capsule shape workspace as task. This improves the using ratio and efficiency of the workspace of PRPM. A 3D printed prototype also has been carried out.**

Index Terms - parallel mechanism; reconfigurable; kinematics; performance indexes; task-oriented.

I. INTRODUCTION

Due to potential industrial applications, attention has been attracted by lower-mobility parallel mechanisms, as they are easier to control than 6-DOF parallel mechanisms. Previous studies on lower-mobility parallel mechanism usually concentrate on fixed structural analysis, such as Tsai[1], Joshi[2], Qu[3] and Zhao[4]. However, with the practical applications of parallel mechanism are getting increasingly important, a mechanism usually need to meet more than one task. Suitable structural parameters should be used to fit specific task requirements. Based on this demand, parameter reconfigurable structure can be applied to parallel mechanism. In this way, different task performance requirements can be satisfied by reconfiguring mechanism structural parameter. This kind of task-oriented parameter determination issue also can be considered as task planning mechanism design problem, which involves two parts: mechanism design and task planning analysis.

For the mechanism design problem, by applying different design theories, many 3- and 4-DOF lower-mobility parameter reconfigurable parallel mechanisms have been developed. Kong[5] carried out a 3-RER parallel mechanism, which can obtain several kinds of operation modes by reconfiguring joint direction. Similarly, Palpacelli[6] proposed a 3-CPU parallel mechanism, which owns two working modes by adapting proper configuration of universal joint. Balmaceda[7] introduced a novel reconfiguration strategy for a Delta-type parallel mechanism by applying different parameters of fixed base. In addition, Kong[8] raised a type synthesis method of 3DOF multi-mode translational/spherical parallel mechanism with lockable joints to realize parameter reconfiguring. All of these parallel mechanisms have the parameter reconfiguring character, which can fit different using demands. However, detailed analysis, which involves parameter determination based on task required performance is somewhat lacking.

On the other hand, the task planning analysis problem can be considered as dimensional synthesis based on specific requirements. Such as Huang[9] did in their research, which optimize a translational pick-and-place parallel mechanism to achieve minimize condition number. Merlet[10] also raised dimensional synthesis analysis by considering positioning errors of *n* DOF parallel mechanism, which moves within a given workspace. Moreover, not only moving platform's performance[11], but also joint motion range can be considered as task requirement during dimensional synthesis work[12]. However, most of task planning researches focus on fixed limb parameter, variable branch structure, compound joint or optimization. It would be better for manufacturing and controlling if a mechanism could realize self-reconfiguring in a simple way to fit task requirements.

The combination study of these two problems has already been performed by some scholars. Dimensional synthesis based on a 3-translational-DOF parallel mechanism for a desired workspace is performed by Affi[13]. Arakelian[14] enlarged singularity-free workspace by changing different suitable configuration of a 3-DOF planer parallel mechanism. Bai[15] developed optimum design of a spherical parallel manipulators for prescribed workspace. Chablat[16] proposed a design method to determine feasible set of parameters of a 3-RRR parallel robots for a prescribed singularity-free workspace. A constrained optimization formulation aimed at determining a manipulator design so that a prescribed workspace is fully enclosed, which is also well-conditioned with respect to some performance index is presented by Hay[17]. Furthermore, not only workspace requirement but also other performance requirements are considered in design problem such as in [18-20]. Modularity has also been

* This work is supported by National Natural Science Foundation of China (Grant No. 51875033) and China Scholarship Council (Grant No. 201807090080).

978-1-7281-6321-5/19//$31.00 ©2019 IEEE

considered in mechanism design for required workspace[21,22].

In this paper, a parameter reconfigurable parallel mechanism (PRPM) is presented. The PRPM can fit task required performance by changing structural parameter. This paper is organized as follows: First, brief sketch as well as DOF analysis of the proposed parallel mechanism are presented in section II. Then, PRPM theoretical analysis model, which includes kinematics solutions and Jacobian matrices is established in section III. Performances which include dexterity, stiffness, workspace, singularity are analyzed in section IV. Finally, task planning analysis fits for specific requirement is raised in section V. Conclusions are presented in section VI.

II. Description of PRPM

A. Assembly Structure

The sketch of a parameter reconfigurable parallel mechanism is shown in Figure 1. The mechanism involves two parts: base part and platform part. The base part consists of a fixed base, a reconfigurable base and four motion branches, which is shown in Figure 1(a). The four branches have the same structure (one prismatic joint P, two rotational joints R) and dimension parameters. Prismatic joints marked by A_i are driven by four linear motors and move synchronously with same driving parameters. Fixed coordinate frame *O-xyz* is attached at the midpoint of fixed base with A_1A_4 as *x* axis and A_2A_3 as *y* axis, *z* axis vertical. Four revolute joint axis of each branch are parallel to plane *xoy*. The platform part involves a moving platform and four motion branches, which is shown in Figure 1(b). The four branches have the same structure (one prismatic joint P, two universal joints U). Platform part locates on base part by using prismatic joints as actuators and A_iB_i(i=1-4) as guide rails. The moving platform $D_1D_2D_3D_4$ shapes as a square, where moving coordinate frame *O'-x'y'z'* is attached at the midpoint. *x'* axis coincides with D_1D_4 and *y'* axis coincides with D_2D_3. *z'* axis vertical. One of each universal joint axis which is connected with moving platform is parallel to *xoy* plane. Through this configuration, the mechanism's workspace volume, stiffness and dexterity can fit a desired task by changing the position of reconfigurable base.

B. Operation Strategy

As mentioned in assembly structure section, PRPM can realize base part reconfiguring according to different tasks. The reconfigurable base should be relocated every time task performance is changed. The working mode of PRPM can be divided into reconfiguring operation and working operation. The two operation strategies are shown below: (i=1-4)

Reconfiguring operation: When reconfiguring base part, l_i is needed to set as l_i=0 firstly, so as to simplify the control strategy. Then prismatic joints A_i should be actuated simultaneously in order to construct $\angle B_iA_iO$ (namely, PRPM structural angle θ) to a specific value. Lastly, prismatic joints A_i would be locked to proceed to working operation.

Working operation: After joints A_i and reconfigurable base are fixed, PRPM can be switched to working operation by applying C_i and A_iB_i as actuated prismatic joints and guide rails respectively.

Given the above, working mode changing can be simply achieved by reconfiguring PRPM base part in proper positions. l_i, A_i, C_i and A_iB_i are defined in detail in section III. The value determination method of θ is discussed in section V.

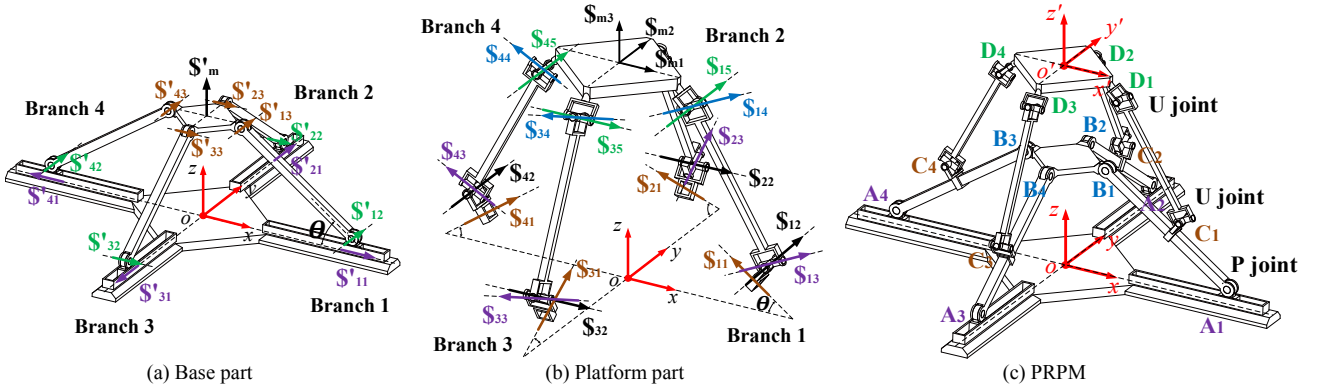

(a) Base part (b) Platform part (c) PRPM

Fig. 1 Sketch of parameter reconfigurable parallel mechanism

C. DOF Analysis

This section performed the moving platform's DOF analysis based on screw theory[23]. The basis twist system of branches 1-4 are given in (1), directions are shown in Figure 1(b). Set c=cosθ, s=sinθ. θ is the angle between A_iB_i and fixed base, also called structural angle in this paper. i=1 or 4, j=2 or 3.

Then, reciprocal screws of (1) should be calculated to obtain constraint screws of branches. The result is shown as (2), in which $m'_i m_i + n'_i n_i = 0$ (i=1-4).

$$
\begin{cases}
\$_{i1} = (0 \quad 0 \quad 0; (-1)^i c \quad 0 \quad s)^{\mathrm{T}}; \\
\$_{i2} = (0 \quad 1 \quad 0; A_{i1} \quad 0 \quad C_{i2})^{\mathrm{T}}; \\
\$_{i3} = (m_i \quad 0 \quad n_i; \ldots \\
\qquad \ldots A_{i3} \quad B_{i3} \quad C_{i3})^{\mathrm{T}}; \\
\$_{i4} = (m_i \quad 0 \quad n_i; \ldots \\
\qquad \ldots A_{i4} \quad B_{i4} \quad C_{i4})^{\mathrm{T}}; \\
\$_{i5} = (0 \quad 1 \quad 0; A_{i5} \quad 0 \quad C_{i5})^{\mathrm{T}};
\end{cases}
\begin{cases}
\$_{j1} = (0 \quad 0 \quad 0; 0 \quad (-1)^{j+1} c \quad s)^{\mathrm{T}}; \\
\$_{j2} = (1 \quad 0 \quad 0; 0 \quad B_{j2} \quad C_{j2})^{\mathrm{T}}; \\
\$_{j3} = (0 \quad m_j \quad n_j; \ldots \\
\qquad A_{j3} \quad B_{j3} \quad C_{j3})^{\mathrm{T}}; \\
\$_{j4} = (0 \quad m_j \quad n_j; \ldots \\
\qquad \ldots A_{j4} \quad B_{j4} \quad C_{j4})^{\mathrm{T}}; \\
\$_{j5} = (1 \quad 0 \quad 0; 0 \quad B_{25} \quad C_{25})^{\mathrm{T}};
\end{cases} \tag{1}
$$

$$\begin{cases} \$_1^{\mathrm{r}} = (0 \quad 0 \quad 0; m'_1 \quad 0 \quad n'_1)^{\mathrm{T}}; \\ \$_2^{\mathrm{r}} = (0 \quad 0 \quad 0; 0 \quad m'_2 \quad n'_2)^{\mathrm{T}}; \\ \$_3^{\mathrm{r}} = (0 \quad 0 \quad 0; 0 \quad m'_3 \quad n'_3)^{\mathrm{T}}; \\ \$_4^{\mathrm{r}} = (0 \quad 0 \quad 0; m'_4 \quad 0 \quad n'_4)^{\mathrm{T}}; \end{cases} \tag{2}$$

Obviously, all constraint screws ($\$_i^{\mathrm{r}}$, i=1-4) of moving platform belong to pure constraint couples. 4 constraint screws are included in constraint system, while system rank equals to 3. Therefore, the modified formula G-K criterion (3)[23] can be applied to calculate the DOF of moving platform.

$$M = d(n-j-1)+\sum_{i=1}^{j} f_i + v \tag{3}$$

In equation (3), the value of DOF is denoted by M; mechanism's order is denoted by d, where d=6-λ and λ represents public constraints number; the components number of mechanism is denoted by n; j stands for the number of joints; the DOF of ith joint is represented by f_i; v stands for redundant constraints number when public constraints are removed. Therefore, DOF of PRPM moving platform can be solved: M=6×(10-12-1)+20+(4-3)=3.

The twists of moving platform can be obtained by calculating reciprocal screws of (2), which is shown as $\$_{\mathrm{mi}}$ (i=1-3) in equation (4). Thus, pure translational motion can be realized by moving platform, which directs along x, y, z axis.

$$\begin{cases} \$_{\mathrm{m1}} = (0 \quad 0 \quad 0; 1 \quad 0 \quad 0)^{\mathrm{T}}; \\ \$_{\mathrm{m2}} = (0 \quad 0 \quad 0; 0 \quad 1 \quad 0)^{\mathrm{T}}; \\ \$_{\mathrm{m3}} = (0 \quad 0 \quad 0; 0 \quad 0 \quad 1)^{\mathrm{T}}; \end{cases} \tag{4}$$

Meanwhile, reconfigurable base's DOF can be worked out easily, which is a single z axis translational motion (reconfigurable base twist $\$'_{\mathrm{m}}$=(0 0 0;0 0 1)$^{\mathrm{T}}$, other branch twists are shown as Figure 1(a)). To sum up 2.3, pure translational motion along x, y, z can be realized by the moving platform of PRPM. The structure parameters can be changed by reconfiguring base part.

III. Kinematic Analysis

The proposed mechanism's driving parameters and moving platform's position parameters can be acquired as (l_1, l_2, l_3, l_4) and (x, y, z) respectively. Other parameters are shown in Figure 2. Then, the kinematics model of PRPM should be established, which is used as basis for kinematic analysis.

By considering the DOF characteristic, orientation angles α β γ all equal to zero. Thus the rotation matrix ${}^0_1\boldsymbol{R}(\alpha, \beta, \gamma)$ and pose transformation matrix T of PRPM can be obtained as equation (5),

$${}^0_1\boldsymbol{R}(\alpha, \beta, \gamma) = diag[1,1,1]; \quad \boldsymbol{T} = \begin{pmatrix} {}^0_1\boldsymbol{R}(\alpha, \beta, \gamma) & {}^0\boldsymbol{O}' \\ 0 & 1 \end{pmatrix}; \tag{5}$$

where ${}^0\boldsymbol{O}'=(x,y,z)^{\mathrm{T}}$ represents the coordinates of moving frame's origin in fixed frame. So coordinates of $\mathrm{D_i}$ in fixed frame can be calculated by ${}^0\mathrm{D_i} = T\cdot{}'\mathrm{D_i}$ (i=1-4). Thus, ${}^0\mathrm{D_i}$ as well as ${}^0\mathrm{C_i}$ are shown in equation (6), (i=1-4)

$$\begin{cases} {}^0\mathrm{C_1} = (R-cl_1, 0, sl_1); \quad {}^0\mathrm{C_2} = (0, R-cl_2, sl_2); \\ {}^0\mathrm{C_3} = (0, -R+cl_3, sl_3); \quad {}^0\mathrm{C_4} = (-R+cl_4, 0, sl_4); \\ {}^0\mathrm{D_1} = (x+r, y, z); \quad {}^0\mathrm{D_2} = (x, y+r, z); \\ {}^0\mathrm{D_3} = (x, y-r, z); \quad {}^0\mathrm{D_4} = (x-r, y, z); \end{cases} \tag{6}$$

where c=cosθ, s=sinθ, R and r denote the circumradius of fixed base and moving platform respectively. Therefore, PRPM's length constraint equations can be obtained as follows,

$$\left\| {}^0\mathrm{C_i}\,{}^0\mathrm{D_i} \right\| = l; \ (\mathrm{i}=1-4) \tag{7}$$

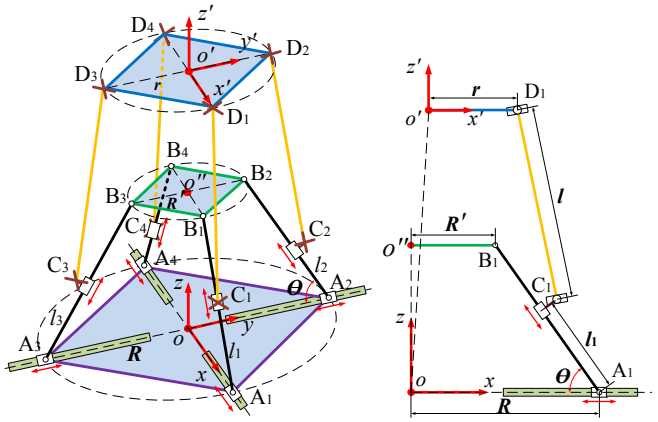

Fig. 2 Vector diagram of the mechanism

A. Inverse Solution

For PRPM, inverse solution is solving (l_1, l_2, l_3, l_4) after (x, y, z) is known. Equations (8a-d) can be obtained by squaring both sides of equation (7)'s equal signs.

$$\begin{cases} (R-cl_1-x-r)^2 + y^2 + (sl_1-z)^2 = l^2 & \text{(8a)} \\ (R-cl_2-y-r)^2 + x^2 + (sl_2-z)^2 = l^2 & \text{(8b)} \\ (-R+cl_3-y+r)^2 + x^2 + (sl_3-z)^2 = l^2 & \text{(8c)} \\ (-R+cl_4-x+r)^2 + y^2 + (sl_4-z)^2 = l^2 & \text{(8d)} \end{cases}$$

The inverse solution can be obtained as equation (9) by simply solving equations 8(a-d). Among equation (9), multinomial coefficients of x, y, z and constant terms are denoted by f_{ij} (i=1-4, j=1-4). Considering mechanism's structure, there will be only one set of inverse solution.

$$l_{\mathrm{i}} = xf_{\mathrm{i1}} + yf_{\mathrm{i2}} + zf_{\mathrm{i3}} + f_{\mathrm{i4}}; \ (\mathrm{i}=1-4) \tag{9}$$

B. Forward Solution

Forward kinematic problem for this work is to solve x, y, z after knowing l_1, l_2, l_3, l_4. We can get equations (10a-c) by making subtraction operations (8a)-(8d), (8b)-(8d), (8c)-(8d) on both sides of equal signs. These three equations constitute a linear system in the three unknowns x, y, z, that is easy to solve and provides directly the solutions. $f_{1\text{-}3}$, $g_{1\text{-}3}$, $h_{1\text{-}3}$, $k_{2\text{-}3}$, are used to denote the polynomial coefficients in (10a-c). p=(θ, R, r), q_1=(l_1, l_4), q_2=(l_2, l_4), q_3=(l_3, l_4).

$$\begin{cases} f_1(p,q_1)x+g_1(\theta,q_1)z+h_1(p,q_1)=0 & \text{(10a)} \\ f_1(p,l_4)x+k_2(p,l_2)y+g_2(\theta,q_2)z+h_2(p,q_2)=0 & \text{(10b)} \\ f_1(p,l_4)x+k_3(p,l_3)y+g_3(\theta,q_3)z+h_3(p,q_3)=0 & \text{(10c)} \end{cases}$$

C. Jacobian Matrix

For PRPM, equation (11) shows the relation between input and output velocities. Input and output velocities are the derivative of input (l_1, l_2, l_3, l_4) and output (x, y, z) with respect to time, which are denoted by $\dot{l}_1, \dot{l}_2, \dot{l}_3, \dot{l}_4$ and $\dot{x}, \dot{y}, \dot{z}$ respectively. $\boldsymbol{J}_I$ and $\boldsymbol{J}_F$ are inverse Jacobian matrix and forward Jacobian matrix respectively.

$$\boldsymbol{J}_I\left[\dot{l}_1,\dot{l}_2,\dot{l}_3,\dot{l}_4\right]^{\mathrm{T}}+\boldsymbol{J}_F\left[\dot{x},\dot{y},\dot{z}\right]^{\mathrm{T}}=0 \qquad (11)$$

To calculate the elements of $\boldsymbol{J}_I$ and $\boldsymbol{J}_F$, the derivative with respect to time should be performed on both sides of equations (8a-d)'s equal signs. The coefficients of $\dot{l}_1, \dot{l}_2, \dot{l}_3, \dot{l}_4$ and $\dot{x}, \dot{y}, \dot{z}$ are written as matrix form shown in (12), which denoted by j_i (i=1-4) and j_{ab} (a =1-4, b=1-3) respectively.

$$\boldsymbol{J}_I=\begin{pmatrix} j_1 & 0 & 0 & 0 \\ 0 & j_2 & 0 & 0 \\ 0 & 0 & j_3 & 0 \\ 0 & 0 & 0 & j_4 \end{pmatrix};\ \boldsymbol{J}_F=\begin{pmatrix} j_{11} & j_{12} & j_{13} \\ j_{21} & j_{22} & j_{23} \\ j_{31} & j_{32} & j_{33} \\ j_{41} & j_{42} & j_{43} \end{pmatrix}; \qquad (12)$$

Then, the overall Jacobian matrix $\boldsymbol{J}$ of PRPM can be obtained as (13).

$$\boldsymbol{J}=\boldsymbol{J}_I^{-1}\cdot\boldsymbol{J}_F \qquad (13)$$

IV. Performance Analysis

In this section, performance analysis of PRPM including stiffness, dexterity, workspace and singularity is performed. The analysis shows the operational performance of PRPM, also can be used as a basis for task planning analysis. Parameters are set as follows: r=35, l=70, R'=24, L=70, where L denotes the length of guide rail A_iB_i. That is, the maximum stroke of C_i. R' denotes circumradius of reconfigurable base as shown in Figure 2. Thus R=R'+cosθ.

A. Dexterity and Stiffness

Dexterity and stiffness are important performance indexes to measure mechanism's operation ability. They reflect the relationship between input and output, while dexterity focuses on motion accuracy and stiffness evaluates mechanism's operational stability. Generally, condition number k is used as the indicator of dexterity, which can be obtained by taking square root of the ratio among extreme eigenvalues of stiffness matrix. The following equation is shown as (14), where λ_{max} and λ_{min} stand for the maximum and minimum eigenvalues of stiffness matrix respectively.

$$k=\sqrt{\lambda_{max}/\lambda_{min}} \qquad (14)$$

As for stiffness matrix $\boldsymbol{K}$ of a parallel mechanism, it can be obtained by equation (15)[24]:

$$\boldsymbol{K}=\boldsymbol{J}^{\mathrm{T}}\boldsymbol{K}_J\boldsymbol{J} \qquad (15)$$

in which $\boldsymbol{K}_J$ is the actuated joints' stiffness matrix and equals to $diag[h_1,\ldots,h_i]$. In this paper, each of the proposed mechanism's joint is seen as an elastic component, h_i denotes the stiffness of actuator l_i. Here, h_i is set to 100 KN/m[25,26] (i=1-4).

The mechanism's condition number distribution diagram on a given z coordinate (z=100) while structural angle θ=60° is plotted in Figure 3. Meanwhile, distribution diagrams of stiffness are plotted in Figures 4. As an illustrative example, Figures 4(a)-(d) are four sets of stiffness distribution diagrams among z directions as θ=60°.

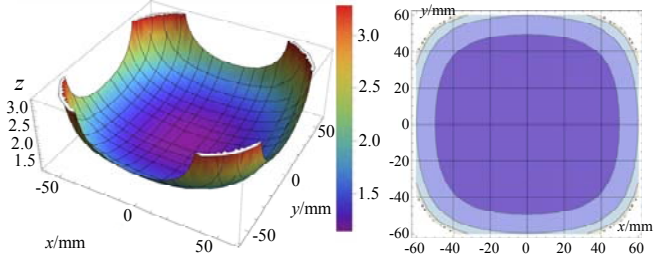

(a) Stereogram (b) Planar graph

Fig. 3 Condition number on the specific xoy plane cross section

From Figure 3 we can know that, the low value area (1.0<k<1.5) can cover most range of workspace in this cross section. Due to the value of condition number k being the best at 1 and always greater than or equal to 1, the dexterity of PRPM in this paper can satisfy most desired applications.

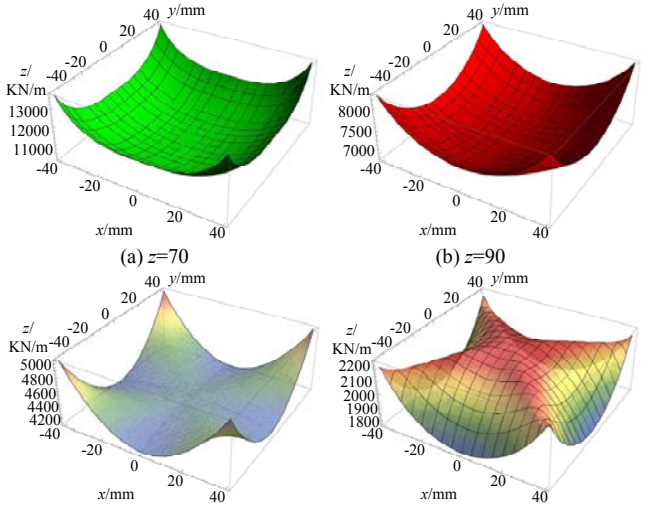

(a) z=70 (b) z=90

(c) z=110 (d) z=130

Fig. 4 Stiffness distribution on the specific xoy plane cross section

From Figures 4 we can find out that PRPM can realize average stiffness distribution in the permitted workspace. As z coordinate getting larger, the stiffness gets lower. The average value of stiffness among the whole workspace can reach 6000KN/m, which is fully capable for different working environments.

B. Workspace and Singularity

Workspace of a parallel mechanism is the motion range that moving platform can reach, which can be used for mechanism performance evaluation. By reconfiguring base part, the workspace of PRPM can satisfy different required tasks. In addition, the study of workspace is closely connected with singularity. Moving platform is more likely to lose balance or DOF under singularity positions because of the

complex structure of parallel mechanism. It would be dangerous for both mechanism and operator if singularity is involved in workspace. Thus, both workspace and singularity are important indicators to examine mechanism's performance.

1) Workspace Analysis:

For orientation angles α, β, γ of PRPM are all equal to zero, orientation workspace is not included in this research. Moreover, due to the location of reconfigurable base can be changed, three typical values of structural angle are chosen as examples during workspace analysis.

Considering the limb interference and actuated joint motion range, PRPM's workspace during structural angle equals 30° (θ=30°) is shown in Figure 5(a). Similarly, workspaces at θ=45° and θ=60° are shown in Figures 5(b) and 5(c) to verify the correctness and different conditions of mechanism's workspace. Areas are colored as yellow.

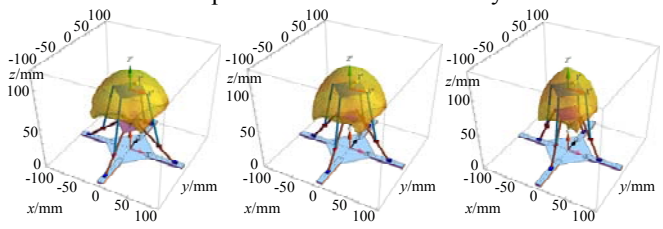

(a) θ=30° (b) θ=45° (c) θ=60°

Fig. 5 Workspaces in different conditions

As Figure 5 shows, all the workspaces under different situations are symmetrical with respect to planes *xoz* and *yoz*, which are correspond with the structure of PRPM. The shape of workspace likes an arc cone. When the structural angle is low (around 30°), the shape of workspace is flat. As structural angle becoming larger, the workspace's volume gets bigger and the range reaches $x \in [-50, 50]$, $y \in [-50, 50]$, $z \in [50, 130]$. As structural angle continue becoming larger, the shape of workspace gets taller and thinner. During structural angle's changing, mechanism's workspace can cover a large range along horizontal and vertical directions. Workspace's shape changing can also satisfy different required tasks.

2) Singularity Analysis:

A parallel mechanism's singularity position can be acquired by correlation parameters of Jacobian matrices. All possible singularity positions can be worked out by applying determinant arithmetic upon $\boldsymbol{J}_I$ and $\boldsymbol{J}_F$ [27,28]. Considering PRPM however, the determinant calculation process is too complex, which would lead to indirect and complicated results. Therefore, the Grassmann Line Geometry method can be used to illustrate all the singularity situations of PRPM. In this work, singularity occurs when the constraint system rank of PRPM is less than 3. In other words, at least three wrenches should be linearly dependent, which are provided by branches. A singularity condition list is shown as Figure 7. The square denotes moving platform. Line segments connect with the platform denote limbs C_iD_i (i=1-4). The directions of wrenches are denoted by arrows. To be noticed, the limb/platform interference situations are not considered.

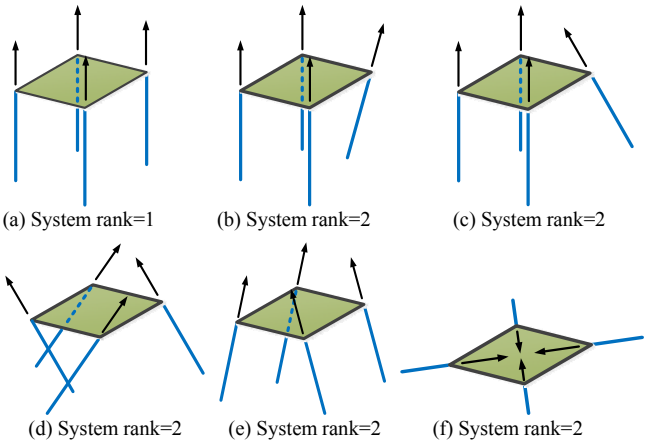

(a) System rank=1 (b) System rank=2 (c) System rank=2

(d) System rank=2 (e) System rank=2 (f) System rank=2

Fig. 6 PRPM singularity conditions

We can see from Figure 6 that, the positions between motion branches and moving platform would cause possible singularity conditions. PRPM singularity occurs when wrench system's rank equals to 1 and 2, which are shown in Figure 6(a) and Figures 6(b)-(f) respectively. Only situation Figure 6(a) may occur by considering PRPM's structural and DOF features. With this in mind and simplifying analysis process, we can set $R' \geqq r$ at the mechanism design and manufacturing stage, so as to avoid four driving values (l_i, i=1-4) equal to each other. Moreover, on account of PRPM is a redundant actuation parallel mechanism, these singularity conditions also can be prevented in advance by controlling redundant actuator properly[29,30].

V. Task Planning Analysis

Due to the characteristic of structural variability by reconfiguring PRPM's base part (changing structural angle), a task planning analysis of PRPM is presented in this section. It can be seen as the determination of structural parameter, which fits for a request task. This also can be considered as user-defined PRPM working mode.

A. Task-oriented Structural Angle Determination

The first thing that a task should be fitted by parallel mechanism is the workspace volume. If the task workspace volume cannot be fully contained by a parallel mechanism's workspace in the first place, then the mechanism cannot satisfy the task requirements. Since PRPM's structural angle θ can be changed, PRPM can use different workspaces to contain task workspace. Due to PRPM's structure, different workspaces can be combined to contain task workspace with specific range of θ. Therefore, task-oriented structural angle range can be calculated by simply applying kinematics model of PRPM. Specific steps are as follows:

1) Acquiring task required workspace (w_t). Geometric limiting points of w_t should be defined as F_n. F_n are a set of points where the midpoint of moving platform can reach, when some of actuated prismatic joints C_i reach limit value.

2) Substituting F_n's coordinate values into inverse solution equation (8). l_i are set to L_{max} or L_{min}, where L_{max} and L_{min} denote the maximum and minimum driving values

respectively. Several sets of structural angle values θ_i (i=1-n) can be worked out by solving the equations.

3) On account of the characteristic of PRPM's workspace, the task-oriented range of structural angle is determined as [θ_{imin}, θ_{imax}], in which θ_{imin} and θ_{imax} denote the minimum and maximum values of θ_i.

4) By applying structural angle as [θ_{imin}, θ_{imax}], PRPM's actual workspace (w_a) should be checked if w_t can be fully contained. If w_t can be contained by w_a, task workspace volume can be satisfied by PRPM. If not, additional geometric limiting points should be added on w_t, and proceed steps 2 and 3 again. If the solution of structural angle is beyond permitted range [15°, 75°], then PRPM cannot fulfill the task.

The above structural angle determination method steps are formed as flow chart, which is shown in Figure 7.

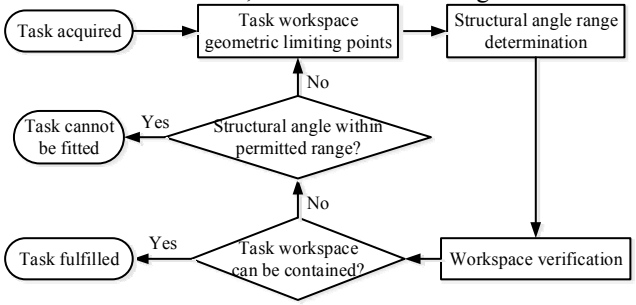

Fig. 7 Flow chart of structural angle determination method

B. *Example Verification*

Here is the demonstration of the structural angle determination method. Suppose a w_t is given as Figure 8 and task planning analysis of PRPM is carried out in this section.

The given w_t's shape is a capsule, which is a combination of two spheres and one cylinder. The cylinder's geometric center is located at (0,0,90) in Cartesian coordinate system. The height of cylinder is along z direction and equals to 40mm. The radius of cylinder equals to 20mm. The two spheres' centers locate at the two centers of top (0,0,110) and bottom (0,0,70) surfaces of the cylinder respectively. The radiuses of two spheres also equal to 20mm. As a consideration of w_t's structure characteristic, we shall establish two geometric limiting points at the top and bottom of w_t respectively, that is F_1(0,0,130) and F_{18}(0,0,50). Eight points are established on the connection circles between sphere and cylinder at top and bottom surfaces respectively, which are $F_6(-10\sqrt{2}, 10\sqrt{2}, 110)$, $F_7(-10\sqrt{2}, -10\sqrt{2}, 110)$, $F_8(10\sqrt{2}, -10\sqrt{2}, 110)$, $F_9(10\sqrt{2}, 10\sqrt{2}, 110)$ at top and $F_{10}(-10\sqrt{2}, 10\sqrt{2}, 70)$, $F_{11}(-10\sqrt{2}, -10\sqrt{2}, 70)$, $F_{12}(10\sqrt{2}, -10\sqrt{2}, 70)$, $F_{13}(10\sqrt{2}, 10\sqrt{2}, 70)$ at bottom. Eight points are also established on the midpoint of arc $\overset{\frown}{F_1F_6}$, $\overset{\frown}{F_1F_7}$, $\overset{\frown}{F_1F_8}$, $\overset{\frown}{F_1F_9}$, $\overset{\frown}{F_{18}F_{10}}$, $\overset{\frown}{F_{18}F_{11}}$, $\overset{\frown}{F_{18}F_{12}}$, $\overset{\frown}{F_{18}F_{13}}$, which are $F_2(-10,10,110+10\sqrt{2})$, $F_3(-10,-10,110+10\sqrt{2})$, $F_4(10,-10,110+10\sqrt{2})$, $F_5(10,10,110+10\sqrt{2})$, $F_{14}(-10,10,70-10\sqrt{2})$, $F_{15}(-10,-10,70-10\sqrt{2})$, $F_{16}(10,-10,70-10\sqrt{2})$, $F_{17}(10,10,70-10\sqrt{2})$ respectively. w_t's diagrams along x-y, x-z, y-z cross-sectional are shown in Figures 8(a)-(c). w_t's 3D diagram is shown in Figure 8(d).

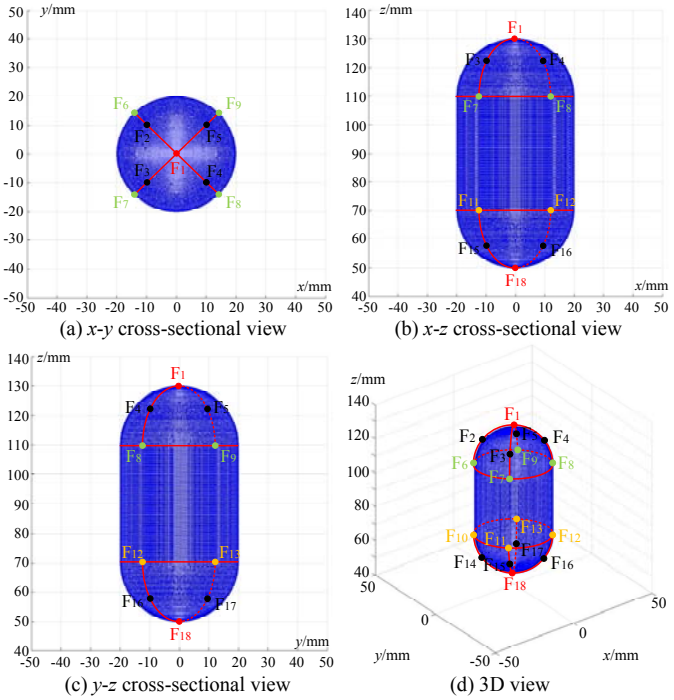

(a) x-y cross-sectional view (b) x-z cross-sectional view

(c) y-z cross-sectional view (d) 3D view

Fig. 8 Sketch maps of w_t

According to structural angle determination method, joint C_i (i=1-4) should reach extreme driving value at F_i (i=1-18). For instance, joint C_1 in branch 1 and joint C_2 in branch 2 reach maximum and minimum driving values, when center of moving platform locates at F_1, F_3, F_7 and F_{13}, F_{17}, F_{18} respectively. Next, the coordinate values of F_1, F_3, F_7 and $l_i=L_{max}=L$ should be substituted into equation (8). θ can be worked out as 62.73°, 61.98°, 60.03° respectively. The coordinate values of F_{13}, F_{17}, F_{18} and $l_i=L_{min}=0$ should also be substituted into equation (8). θ can be worked out as 57.25°, 51.24°, 54.62° respectively. For each branch, ten F_i are needed to consider. Specifically, five points which let corresponding branch reaches maximum driving value, and the rest of five points which let the branch reaches minimum driving value. The calculation results of structural angle at each F_i and corresponding branch's driving status are tabulated as Table 1. According to above section, the task-oriented structural angle range is $\theta \in$[51.24°, 62.73°]. Comparison diagrams between w_t and w_a under different structural angle situations are shown in Figures 11-14, in which w_t is colored as dark blue, w_a are colored as light blue, red, yellow when θ=62.73°, θ=51.24°, $\theta \in$[51.24°, 62.73°] respectively.

TABLE I
Θ CALCULATION RESULTS AT EACH POINT F_i

	Maximum driving value (Branch 1-4)				Minimum driving value (Branch 1-4)				θ value(°)
	1	2	3	4	1	2	3	4	
F_1	√	√	√	√					62.73
F_2	√		√						61.98
F_3	√	√							61.98
F_4		√		√					61.98
F_5			√	√					61.98

F_6	√		√						60.03
F_7	√	√							60.03
F_8		√		√					60.03
F_9			√	√					60.03
F_{10}						√		√	57.25
F_{11}							√	√	57.25
F_{12}					√		√		57.25
F_{13}					√	√			57.25
F_{14}						√		√	51.24
F_{15}							√	√	51.24
F_{16}					√		√		51.24
F_{17}					√	√			51.24
F_{18}					√	√	√	√	54.62

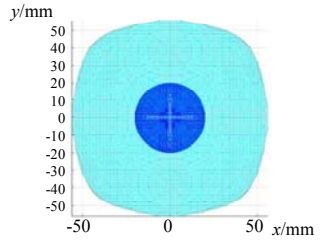

(a) *x*-*y* cross-sectional view

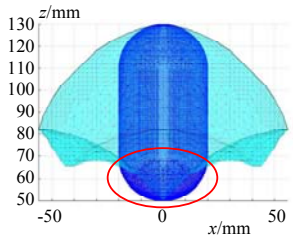

(b) *x*-*z* cross-sectional view

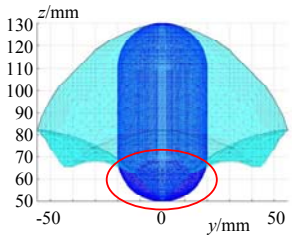

(c) *y*-*z* cross-sectional view

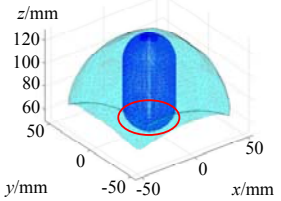

(d) 3D view

Fig. 9 Comparison diagram between w_t and w_a when θ=62.73°

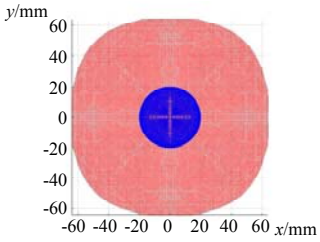

(a) *x*-*y* cross-sectional view

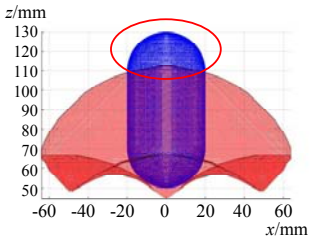

(b) *x*-*z* cross-sectional view

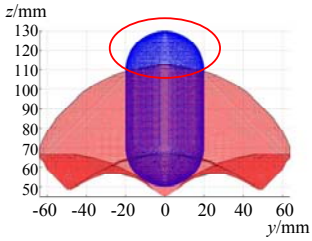

(c) *y*-*z* cross-sectional view

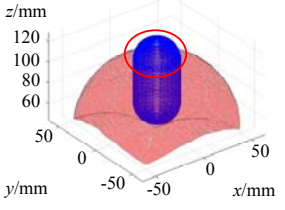

(d) 3D view

Fig. 10 Comparison diagram between w_t and w_a when θ=51.24°

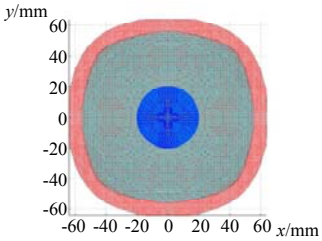

(a) *x*-*y* cross-sectional view

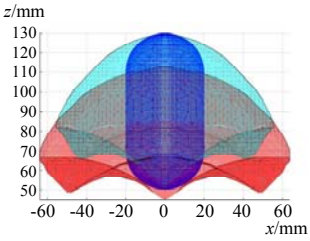

(b) *x*-*z* cross-sectional view

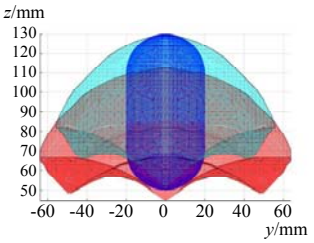

(c) *y*-*z* cross-sectional view

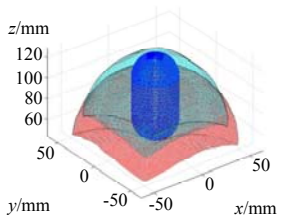

(d) 3D view

Fig. 11 Comparison diagram between w_t and w_a when combining θ=51.24° and θ=62.73°

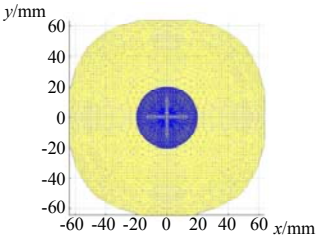

(a) *x*-*y* cross-sectional view

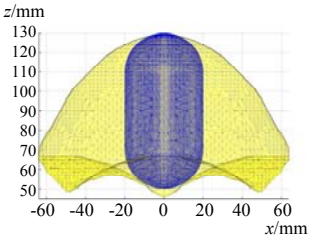

(b) *x*-*z* cross-sectional view

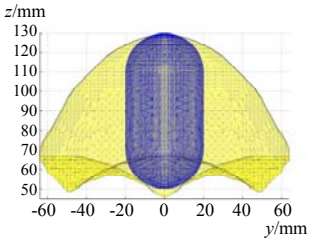

(c) *y*-*z* cross-sectional view

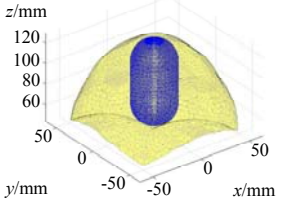

(d) 3D view

Fig. 12 Comparison diagram between w_t and w_a when $\theta \in$ [51.24°, 62.73°]

According to θ calculation result in Table 1, θ_{imin}=51.24°, θ_{imax}=62.73°, i=1-18. As shown in Figures 9 and 10, w_t cannot be satisfied by w_a when applying $\theta=\theta_{imin}$ and $\theta=\theta_{imax}$. The exceeding part of w_t, which cannot be contained by w_a is marked by red curve. But if w_a under $\theta=\theta_{imin}$ and $\theta=\theta_{imax}$ can be combined as one, w_t can be fully contained in w_a, which is shown in Figure 11. Thus, w_a by changing θ among [51.24°, 62.73°] is shown in Figure 12, which step size is 0.03°. As shown in the figure, PRPM's workspace can completely satisfy the task workspace requirement by reconfiguring structural angle from 51.24° to 62.73°.

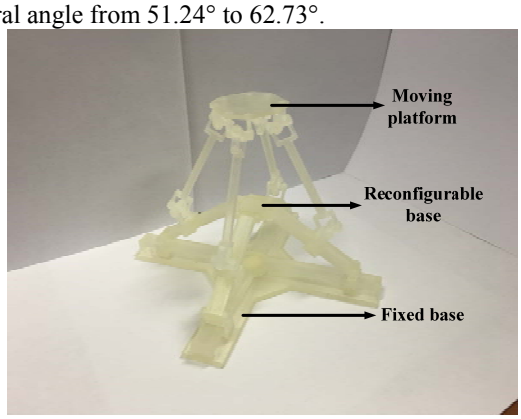

Fig. 13 3D printer prototype of PRPM

Above all, the proposed parameter reconfigurable parallel mechanism owns task-oriented structural design. By reconfiguring base part, the smallest workspace of moving

platform can be obtained to satisfy a corresponding task workspace. Based on the theoretical analysis from sections II to V, a prototype of PRPM has been developed by 3D printer, shown as Figure 13. Multiple operational models can be realized by the prototype. The prototype also shows the manufacturing feasibility of PRPM and proves the correctness of theoretical analysis.

VI. CONCLUSIONS

Kinematic performance and task planning analysis of a parameter reconfigurable parallel mechanism (PRPM) is raised in this work. Major works and conclusions are listed below:

1) By analyzing DOF of PRPM, the correctness of three pure translational motion and variable structural parameter characteristics have been proved.

2) PRPM theoretical analysis model is established, which includes inverse/forward kinematics solutions and Jacobian matrices.

3) Performance indexes including workspace, singularity, dexterity, and stiffness are analyzed, which proved different tasks can be satisfied by performance changing of PRPM.

4) Based on kinematics, task planning analysis of PRPM is carried out. Task-oriented operating model of PRPM has been verified.

REFERENCES

[1] L Tsai, "Kinematics of a three-DOF platform with three extensible limbs", *Recent Advances in Robot Kinematics*, pp. 401-410, 1996.

[2] S Joshi, and L Tsai, "Jacobian analysis of limited-DOF parallel manipulators", *Journal of Mechanical Design*, Vol. 124, No. 2, pp. 254-258, 2002.

[3] H Qu, Y Fang, S Guo, and W Ye, "A novel 4-UPU translational parallel mechanism with fault-tolerant configurations", *Proc IMechE Part C: J Mechanical Engineering Science*, Vol. 228, No. 16, pp. 3006-3018, 2014.

[4] J Zhao, Y Fu, K Zhou, and Z Feng, "Mobility properties of a Schönflies-type parallel manipulator", *Robotics and Computer-Integrated Manufacturing*, Vol. 22, No. 2, pp. 124-133, 2006.

[5] X Kong, "Reconfiguration analysis of a 4-DOF 3-RER parallel manipulator with equilateral triangular base and moving platform", *Mechanism and Machine Theory*, Vol. 98, pp. 180-189, 2016.

[6] M Palpacelli, L Carbonari, G Palmieri, and M Callegari, "Analysis and design of a reconfigurable 3-DoF parallel manipulator for multimodal tasks", *IEEE/Asme Transactions on Mechatronics*, Vol. 20, No. 4, pp. 1975-1985, 2015.

[7] A Balmaceda-Santamaría, E Castillo-Castaneda, and J Gallardo-Alvarado, "A novel reconfiguration strategy of a Delta-type parallel manipulator", *International Journal of Advanced Robotic Systems*, Vol. 13, No. 1, pp. 15, 2016.

[8] X Kong, Y Jin, "Type Synthesis of 3-DOF multi-mode translational/ spherical parallel mechanisms with lockable joints", *Mechanism and Machine Theory*, Vol. 96, No. 2, pp. 323-333, 2006.

[9] T Huang, Z Li, M Li, et al, "Conceptual design and dimensional synthesis of a novel 2-DOF translational parallel robot for pick-and-place operations", *Journal of Mechanical Design*, Vol. 126, No. 3, pp. 449-455, 2004.

[10] J Merlet, and D Daney, "Dimensional synthesis of parallel robots with a guaranteed given accuracy over a specific workspace", *2005 IEEE international conference on robotics and automation*, IEEE, pp. 942-947, Barcelona, Spain, 18-22 April, 2005.

[11] P Huang, J Wang, L Wang, and J Qian, "Dimensional synthesis for 3-PRS mechanism based on identifiability performance", *Chinese Journal of Mechanical Engineering*, Vol. 25, No. 2, pp. 234-240, 2012.

[12] N Rao, and K Rao, "Dimensional synthesis of a spatial 3-RPS parallel manipulator for a prescribed range of motion of spherical joints", *Mechanism and Machine Theory*, Vol. 44, No. 2, pp. 477-486, 2009.

[13] Z Affi, L Romdhane and A Maalej, "Dimensional synthesis of a 3-translational-DOF in-parallel manipulator for a desired workspace", *European Journal of Mechanics*, Vol. 23, No. 2, pp. 311-324, 2004.

[14] V Arakelian, S Briot, V Glazunov, "Increase of singularity-free zones in the workspace of parallel manipulators using mechanisms of variable structure", *Mechanism & Machine Theory*, Vol. 43, No. 9, pp. 1129-1140, 2008.

[15] S Bai, "Optimum design of spherical parallel manipulators for a prescribed workspace", *Mechanism & Machine Theory*, Vol. 45, No. 2, pp. 200-211, 2010.

[16] D Chablat, G Moroz, V Arakelian, et al, "Solution regions in the parameter space of a 3-RRR decoupled robot for a prescribed workspace", *Advances in Robot Kinematics*, Innsbruck, Austria, pp. 357-364, 25-28 June, 2012.

[17] A Hay and J Snyman, "The optimal synthesis of parallel manipulators for desired workspace", *Advances in Robot Kinematics*, Caldes de Malavalla, Spain, pp. 337-346, June 29- July 2, 2002.

[18] O Altuzarra, A Hernandez, O Salgado and J Angeles, "Multiobjective optimum design of a symmetric parallel Schönflies -motion generator", *Journal of Mechanical Design*, Vol. 131, No. 3, pp. 031002, 2009.

[19] S Briot, A Pashkevich and D Chablat, "Optimal technology-oriented design of parallel robots for high-speed machining applications", *IEEE International Conference on Robotics and Automation*, Anchorage, USA, pp. 1155-1161, 3-8 May, 2010.

[20] J Carretero, R Podhorodeski, M Nahon and C Gosselin, "Kinematic analysis and optimization of a new three degree-of-freedom spatial parallel manipulator", *Journal of Mechanical Design*, Vol. 122, No. 1, pp. 17-24, 2000.

[21] Z Bi and L Wang, "Optimal design of reconfigurable parallel machining systems", *Robotics & Computer-Integrated Manufacturing*, Vol. 25, No. 6, pp. 951-961, 2009.

[22] J Merlet, "Determination of the optimal geometry of modular parallel robots", *IEEE International Conference on Robotics and Automation*, Taipei, China, pp. 1197-1202, 14-19 September, 2003.

[23] Z Huang, L Kong, and Y Fang, *Mechanism theory and control of parallel manipulator*, Beijing: China Machine Press, 1997.

[24] G Coppola, D Zhang, and K Liu, "A 6-DOF reconfigurable hybrid parallel manipulator", *Robotics and Computer-Integrated Manufacturing*, Vol. 30, No. 2, pp. 99-106, 2014.

[25] X Liu, Z Jin, and F Gao, "Optimum design of 3-DOF spherical parallel manipulators with respect to the conditioning and stiffness indices", *Mechanism and Machine Theory*, Vol. 35, No. 9, pp. 1257-1267, 2000.

[26] X Liu, *The relationships between the performance criteria and link lengths of the parallel manipulators and their design theory*, Ph.D. thesis, Yanshan University, Qinhuangdao, China, 1999.

[27] Y Fang, and L Tsai, "Feasible motion solutions for serial manipulators at singular configurations", *Journal of Mechanical Design*, Vol. 125, No. 1, pp. 2367-2367, 2003.

[28] C Gosselin, and J Angeles, "Singularity analysis of closed-loop kinematic chains", *IEEE Transactions on Robotics & Automation*, Vol. 6, No. 3, pp. 281-290, 1990.

[29] M Conconi, and M Carricato, "A new assessment of singularities of parallel kinematic chains", *IEEE Transactions on Robotics*, Vol. 25, No. 4, pp. 757-770, 2009.

[30] T Ropponen, and Y Nakamura, "Singularity-free parameterization and performance analysis of actuation redundancy", *IEEE international conference on robotics and automation*, IEEE, pp.806–811, Cincinnati, OH, USA, 1990.